



Cite this: *New J. Chem.*, 2021, 45, 20241

Digestive ripening yields atomically precise Au nanomolecules†

Senthil Kumar Eswaramoorthy  and Amala Dass *

Digestive ripening (DR) is a synthetic method where a polydisperse colloid of metal nanoparticles upon refluxing with a free ligand in a high boiling point solvent gives monodisperse nanoparticles. Brust synthesis is known to form atomically monodisperse thiolate protected gold nanoparticles also known as gold nanomolecules (Au NMs). Unlike the Brust method which gives smaller (1–3 nm) atomically precise nanomolecules, DR has been used only for the synthesis of large nanoparticles (>5 nm) with good monodispersity. In thiolate protected gold nanoparticle Brust synthesis, the yellow colored phase transferred Au(III) solution is converted to a colorless Au(I) mixture after the addition of thiol by forming Au–SR, which is then reduced to form black colored Au NMs. However, in DR, by using the same primary chemicals, the two steps were reversed: the mixture was reduced before the addition of thiol. Here we show that in DR, adding thiol after 2 minutes of reduction gives larger particles (5 nm) as reported, whereas adding thiol 30 seconds after reduction results in smaller particles (<2 nm). In this work, for the first time, DR yields atomically precise Au₂₅(SR)₁₈ and Au₁₄₄(SR)₆₀ NMs. This is reported using two aliphatic thiols – hexanethiol and dodecanethiol – as the protecting ligands. DR was also repeated using an aromatic thiol, 4-*tert*-butyl benzene thiol (TBBT), which yields Au₂₇₉(SR)₈₄ NMs consistent with the Brust method, thereby establishing that both DR and Brust methods lead to the formation of atomically precise Au NMs, regardless of the order of thiol addition and reduction steps.

Received 23rd August 2021,
Accepted 1st October 2021

DOI: 10.1039/d1nj04042a

rsc.li/njc

Introduction

Nanosized metal particles attract huge interest in catalysis, optics, and drug delivery because of their remarkable difference in physical and chemical properties from the respective bulk metals.¹ The usage of nanosized metal particles dates back to the 4th century AD, the Lycurgus cup.² It exhibits unusual optical effects due to the presence of gold and silver nanoparticles. The size of the particle determines its properties. The catalytic properties of noble metals are enhanced when their size is reduced to the nanoscale.^{3,4} The size-controlled synthesis of NPs is achieved by manipulating the synthetic conditions.^{5,6}

Research of monolayer thiol protected gold nanoparticles (Au NPs) has developed significantly since the introduction of the Brust⁷ method. It is a two-phase synthesis (water/toluene) which was later tuned to form atomically monodisperse nanoparticles, also called gold nanomolecules (Au NMs).^{8–11} The first major development in the field was hints of monodispersity evidenced by mass spectrometric studies reported by Whetten *et al.*¹¹ The next major development was the crystal

structure determination of Au₁₀₂(*p*-MBA)₄₄ and Au₂₅(SCH₂CH₂Ph)₁₈ proving the atomically monodisperse nature beyond any doubt.^{8,9} Later, many other crystal structures were reported, especially using bulky ligands such as 4-*tert*-butylbenzene thiol (TBBT)^{12–14} and *tert*-butyl thiol.^{15–17} Various sizes of NMs protected by different thiolate ligands were obtained by introducing some modifications in the Brust method. But, the basic 3 steps are the same in every Brust method: (i) phase transfer, (ii) addition of thiol, and (iii) reduction using a reducing agent.^{7–11,18} In most cases, the basic steps forming the crude mixture involve an etching process to obtain stable sizes.¹⁹

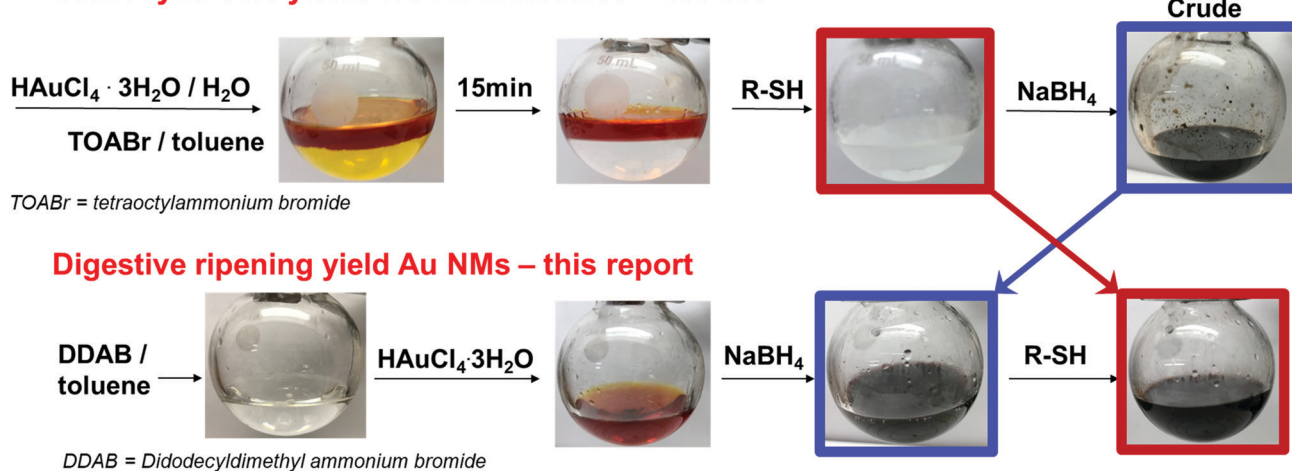
Ostwald ripening, a diffusion-controlled crystal growth process used for the formation of nanoparticles, was proposed in the early to the mid-20th century. In a supersaturated solution, a small change like concentration fluctuation produces the nucleus of a new solid phase which leads to the formation of the nuclei until the degree of supersaturation becomes minimum.²⁰ Then, coalescence occurs in such a way that the particles which have a size larger than the critical size will gain smaller size particles and grow. The theory of Ostwald ripening was introduced in the work of Lifshitz and Slyozof²¹ and further advanced by the work of Wagner,²² together called the LSW theory.

Digestive ripening (DR), which is also known as inverse Ostwald ripening, involves the etching or dissolution of large

Department of Chemistry and Biochemistry, University of Mississippi, Oxford, MS 38677, USA. E-mail: amal@olemiss.edu

† Electronic supplementary information (ESI) available. See DOI: 10.1039/d1nj04042a

Brust synthesis yields NC Au molecules – 1994/96



Scheme 1 Synthetic procedure of the Brust synthesis method yielding nanocrystal gold molecules which were reported in 1994 [ref. 7] and 1996 [ref. 11] directly compared with digestive ripening yielding gold nanomolecules reported in this work.

NPs into smaller, more stable NPs in the presence of excess capping ligands at a high temperature.^{23–25}

DR is one of the commonly used methods for synthesizing various sizes of nanoparticles with size monodispersity in different transition metals.^{25–27} Various factors affecting the monodispersity and properties of the product nanoparticle have been widely studied for this method.^{25–31} The DR method is also used to synthesize monolayer thiol protected Au NPs. But the synthesis of atomically monodisperse nanoparticles using the DR method is not yet achieved. In this report, we demonstrate DR using transmission electron microscopy (TEM) by adding thiol after 2 minutes of reduction which gives larger particles (5 nm) as reported, whereas adding thiol in 30 seconds after reduction results in smaller particles (<2 nm). Thereby, we report that (i) atomic precision can be achieved in DR by reducing the timing (time difference) between the reduction of the mixture and the addition of thiol. (ii) DR yields atomically precise Au₂₅(SR)₁₈ and Au₁₄₄(SR)₆₀ NMs. This is reported using two aliphatic thiols – hexanethiol and dodecanethiol – as the protecting ligands consistent with the reported Au NMs from the Brust method.^{8,32,33} DR was also repeated using an aromatic thiol, TBBT, which yields Au₂₇₉(SR)₈₄ NMs.¹² This is consistent with the reported Au NMs from the Brust method. Mass spectrometric analysis confirms the atomic precision. (iii) The switching of the phase transfer agent to TOABr in DR makes all chemicals (reactant) used for DR and Brust method the same, but the steps are different. Particularly steps 2 and 3 mentioned earlier in the Brust method were reversed in DR, but both pathways lead to the formation of atomically precise Au NMs.

Results and discussion

The step-by-step comparison of the synthetic procedure of Brust and DR methods is shown in Scheme 1. The important difference appears at a distinctive step (highlighted by red and

blue boxes with arrows), where the reduction of the mixture and the addition of thiol steps are reversed. The comparative color change happening in the reactants at each step is evident from the scheme. The Brust method is already known to form atomically precise Au NMs, whereas DR is known to form size monodisperse Au NPs (not atomically monodisperse). Here, DR also leads to the formation of atomically precise Au NMs using the reported synthetic protocols providing unprecedented results as explained below.

Formation of atomic precise small nanoparticles in DR

The DR synthesis was performed as mentioned in Scheme 1. Briefly, the Au salt was dissolved in toluene using a phase transfer agent, followed by reduction, and then the addition of a capping ligand to the mixture. See the Experimental section for more details. Normally in DR, after the reduction of the mixture, the reaction is continued to completion before adding thiol. In the Brust method, the thiol was already present while reducing the mixture. Here, in DR, to obtain smaller gold nanoparticles, we noticed that the timing between the reduction of the mixture and the addition of thiol is crucial. Therefore, the addition of thiol was performed at two time-points: soon after the reduction (30 seconds) and after some time (2 minutes). The transmission electron microscopy (TEM) image (Fig. 1a) of the 30-second DR product shows particles less than 5 nm in size, and their size distribution analysis performed by counting the size of 600 particles provides the value of 1.1 ± 0.3 nm (Fig. 1c). The TEM image of the 2 minute DR product (Fig. 1b) shows comparatively larger monodisperse spheres, and their size distribution analysis performed by counting the size of 400 particles provides the value of 5 ± 0.6 nm (Fig. 1d). The particle size drastically reduced from 5 nm (Fig. 1d) to 1.1 nm when reducing the timing from 2 minutes to 30 seconds. The UV-vis spectra of the 2 minute product shown in the inset of Fig. 1d show a prominent plasmonic band centered at ~ 500 nm, whereas the 30-second

30 seconds

2 minutes

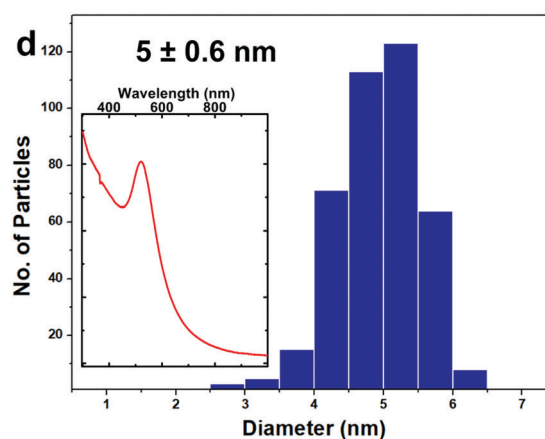
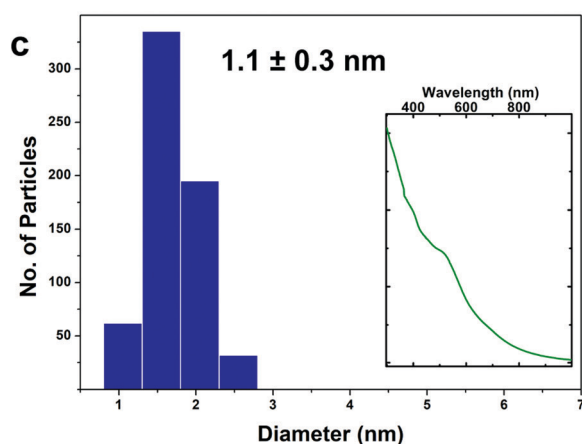
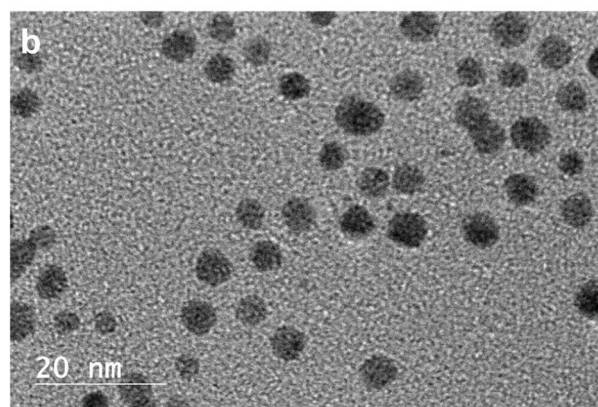
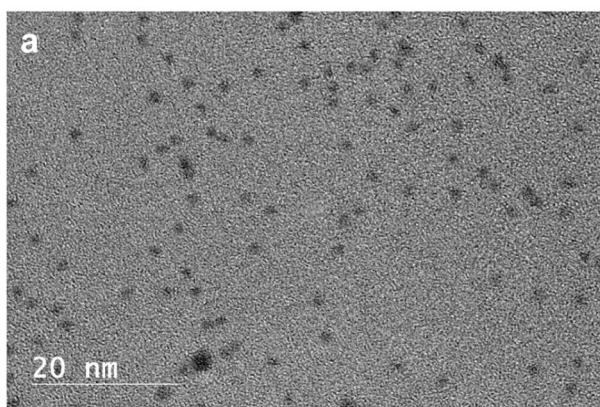


Fig. 1 Addition of thiol after 30 seconds of reduction, (a) TEM image and (c) size distribution plot of its product (UV-vis spectra in the inset). Addition of thiol after 2 minutes of reduction, (b) TEM image and (d) size distribution plot of its product (UV-vis spectra in the inset).

sample (Fig. 1c inset) shows a minute feature in the same region. Therefore, this UV-vis spectrum further confirms the drastic decrease in the size of the resulting product by reducing the timing. The addition of capping agent (thiol) soon after reducing the mixture (30 seconds) stops the aggregation of Au into larger nanoparticles and leads to the formation of particles in the Au nanomolecule regime (1–2 nm).^{34,35} Further refluxing of the mixture makes all the metastable Au nanoclusters into more stable atomically precise Au NMs.

DR yields Au NMs with aliphatic thiols

The DR product was then analyzed using matrix-assisted laser desorption time of flight (MALDI-MS) mass spectrometry using the DCTB matrix.³³ The low and high laser intensity MALDI-MS data exhibit various sizes in the product. With high laser intensity the nanoclusters tend to fragment, but higher laser fluence is needed to ionize all the sizes present in the product. The high laser intensity data of hexanethiol protected Au NMs in Fig. 2a show the presence of two products, namely, at 7 and 30 kDa. The exact mass with high accuracy can be determined using electrospray ionization mass spectrometry (ESI-MS). The ESI-MS spectrum in Fig. 2b predominantly shows 3 sizes of

nanoclusters, namely, Au₂₅(SR)₁₈, Au₁₃₇(SR)₅₆, and Au₁₄₄(SR)₆₀. In Fig. 2b, 17 698 Da and 11 799 Da peaks are observed, representing the 2+ and 3+ charge peaks of Au₁₄₄(SR)₆₀ which has a molecular weight of 35 397 Da. Similarly, the 2+ and 3+ charge states of Au₁₃₇(SR)₅₆ peaks are observed at 16 774 Da and 11 183 Da. The 1+ charge state of Au₂₅(SR)₁₈ at 7034 Da is also observed in Fig. 2b. The same synthesis protocol is repeated for another aliphatic thiol, dodecanethiol. The same 3 sizes are observed in dodecanethiol as shown in Fig. S1 (ESI[†]). Fig. S1a (ESI[†]) shows the MALDI-MS spectra of dodecanethiol protected nanoclusters synthesized using the DR method. The high laser intensity data reveal the formation of 2 sizes, one around 7 kDa and a broad peak at 32 kDa. The low laser intensity data in Fig. S1a (ESI[†]) show the peak of Au₂₅(SR)₁₈, and the adjacent peak is characteristic of MALDI fragmentation of Au₄(SR)₄. The ESI-MS data in Fig. S1b (ESI[†]) showing a 1+ charge state of Au₂₅(SR)₁₈ confirm the same. The broad peak at 32 kDa from MALDI-MS has 2 species which is confirmed by its respective ESI-MS spectra in Fig. S1b (ESI[†]). The 2 species are Au₁₄₄(SR)₆₀ (3+ and 4+ charge state peaks marked in Fig. S1b, ESI[†]) and Au₁₃₇(SR)₅₆ (3+ charge state peak marked in Fig. S1b, ESI[†]). From the extensive research on thiolate protected nanoclusters, the linear chain aliphatic thiol makes a unique

DR yields Au NMs

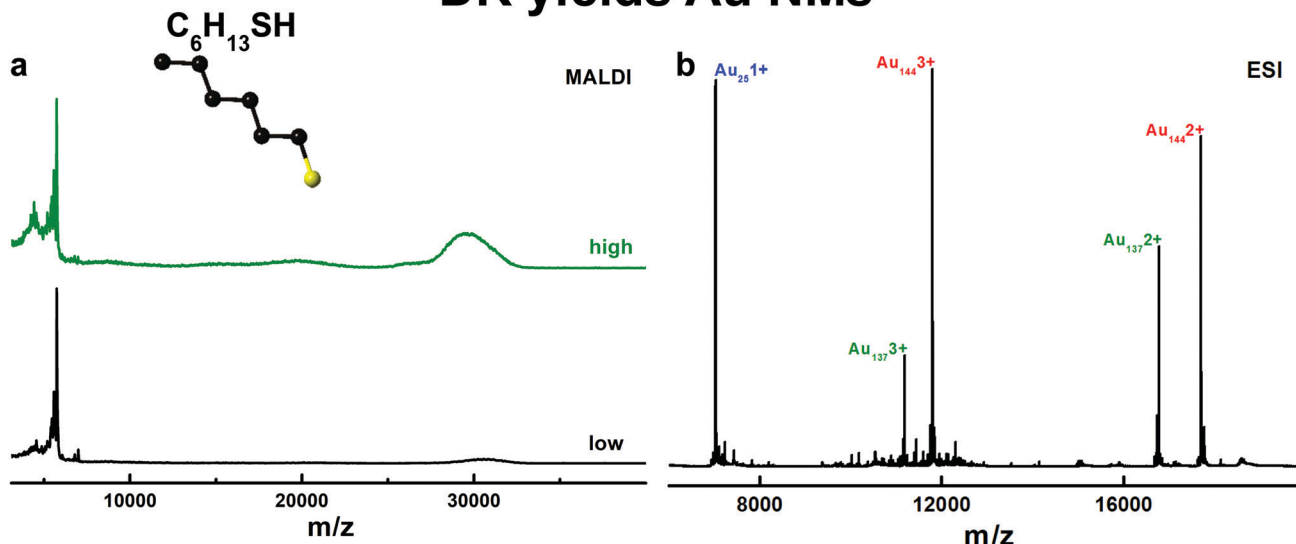


Fig. 2 Mass spectrum of the digestive ripening synthesis product showing atomically precise nanomolecules protected by hexanethiol. (a) MALDI-MS data of the digestive ripening synthesis product showing high intensity (green) and low intensity (black) lasers. (b) ESI-MS data of the same product showing the presence of $\text{Au}_{144}(\text{SR})_{60}$, $\text{Au}_{137}(\text{SR})_{54}$ and $\text{Au}_{25}(\text{SR})_{18}$ species.

series ($\text{Au}_{25}(\text{SR})_{18}$, $\text{Au}_{38}(\text{SR})_{24}$, $\text{Au}_{137}(\text{SR})_{56}$ and $\text{Au}_{144}(\text{SR})_{60}$) from the Brust method of synthesis.^{34–36} The same series containing $\text{Au}_{25}(\text{SR})_{18}$, $\text{Au}_{137}(\text{SR})_{56}$ and $\text{Au}_{144}(\text{SR})_{60}$ is observed in this work using the DR method.

Fig. S2 (ESI[†]) shows the optical properties of Au NMs protected by hexanethiol and dodecanethiol. $\text{Au}_{144}(\text{SR})_{60}$ and $\text{Au}_{137}(\text{SR})_{54}$ do not have prominent optical features in the UV-vis region.^{32,37} But as in Fig. S2 (ESI[†]), both spectra exhibit a small plasmonic resonance feature at ~ 500 nm. It indicates the presence of larger species in the plasmonic range in small amounts.

DR yields Au NMs using an aromatic thiol (TBBT)

The same synthesis protocol was followed with a different thiol, 4-*tert*-butylbenzenethiol (TBBT). Unlike aliphatic thiols, in TBBT, the sulfur atom is attached to the phenyl ring. Additionally, it has a tertiary group attached to the *para* position of the phenyl ring. This gives different electronic, steric, and π - π ligand interaction properties to the product Au NMs.³⁸ As a result, it gives a whole different series of Au NMs.^{38,39} This series is called aromatic series as the sulfur is directly attached to the phenyl ring.³⁸ Fig. 3a shows the MALDI-MS spectrum data of TBBT protected Au NMs. It shows a peak at ~ 62 kDa in low laser intensity (black) corresponding to the $\text{Au}_{279}(\text{SR})_{84}$ species as reported using the Brust method of synthesis.¹² High laser intensity shows the same species, but only gold core mass at ~ 55 kDa. This is because of the removal of surface ligands in the presence of higher laser intensity. The ESI-MS spectrum in Fig. 3b shows the 3+ (22 945 Da), 4+ (17 209 Da) and 5+ (13 767 Da) states of the $\text{Au}_{279}(\text{SR})_{84}$ species.

Isolation of pure Au NMs using size exclusion chromatography (SEC)

DR gives a mixture of Au NM sizes as discussed earlier. SEC is one of the best methods used for the isolation of Au NMs based

on the size.^{40,41} Here, SEC is used to isolate pure Au NMs from the final DR product containing the mixture of sizes. The size separated and purified DR samples can then be compared with the previously reported Brust method using similar purification techniques.^{8,9,12,15–17,32,33,37,42} Fig. S3b and S4b (ESI[†]) show the SEC column during the last stage of separation. Both images (Fig. S3b and S4b, ESI[†]) have two nicely separated bands, first at the bottom, a black band with 30 kDa species having mainly $\text{Au}_{144}(\text{SR})_{60}$, and a second, reddish brown band on the top is pure $\text{Au}_{25}(\text{SR})_{18}$. The SEC isolated MALDI-MS data of hexanethiol protected Au NMs shown in Fig. S5a (ESI[†]) and the corresponding ESI-MS data shown in Fig. S5b (ESI[†]) – the top red spectra showing only the 30 kDa peak in MALDI and the 3+ peak of $\text{Au}_{144}(\text{SR})_{60}$ and $\text{Au}_{137}(\text{SR})_{54}$, confirm the isolation of 30 kDa species. Similarly, the bottom black spectra showing the $\text{Au}_{25}(\text{SR})_{18}$ peak in MALDI-MS data and the 1+ peak of $\text{Au}_{25}(\text{SR})_{18}$ in ESI-MS data confirm the isolation of $\text{Au}_{25}(\text{SR})_{18}$. The UV-vis spectrum of (Fig. S3a, red, ESI[†]) the isolated $\text{Au}_{144}(\text{SR})_{60}$ exhibits no distinctly observed peaks but minor peaks at ~ 510 nm and ~ 700 nm. This is consistent with the previously reported studies and confirms the purity.^{32,42} Similarly, the UV-vis spectrum of $\text{Au}_{25}(\text{SR})_{18}$ (Fig. S3a, black, ESI[†]) shows well defined peaks at 400, 450, and 670 nm and slight shoulder peaks at ~ 575 and ~ 815 nm as previously reported.^{35,36,43}

Likewise, Fig. S6 (ESI[†]) shows the isolation of 30 kDa and 8 kDa dodecanethiol protected Au NMs using MALDI-MS and ESI-MS. Fig. S4a (ESI[†]) confirms the purity of isolation from the UV-vis spectra.^{32,36,42} These results using two different ligands (hexanethiol and dodecanethiol) confirm that DR synthesis produces atomically monodisperse nanomolecules that match with the previously reported Brust synthesis.^{32,36,42}

DR yields Au NMs

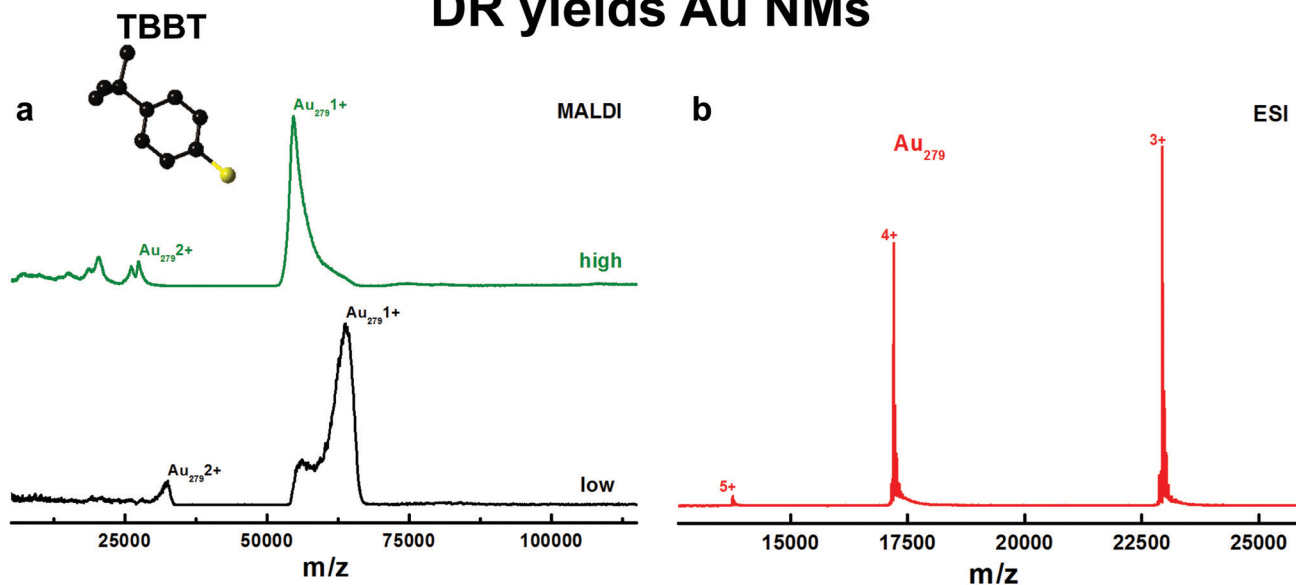


Fig. 3 Mass spectrum confirming the repeatability of digestive ripening yielding atomically precise gold nanomolecules with a rigid secondary ligand (TBBT) where S is directly attached to the phenyl ring. (a) High (green) and low (black) laser intensity MALDI-MS of the digestive ripened product. (b) ESI-MS of the digestive ripened product showing the 3+, 4+ and 5+ charge states of $\text{Au}_{279}(\text{SR})_{84}$.

Mass spectrometry comparison of DR and Brust methods

Samples were prepared using the 2-phase Brust method for comparison purposes. The dodecanethiol protected NMs are synthesized using the Brust method as mentioned in the Experimental section. The MALDI mass spectrum comparison of DR and Brust syntheses, as in Fig. S7 (ESI[†]), shows that they both have 2 distinct peaks at 7 and 32 kDa. Their corresponding ESI-MS data comparison shown in Fig. 4 depicts the 3+ charge state of $\text{Au}_{144}(\text{SR})_{60}$ (13 482 Da) and $\text{Au}_{137}(\text{SR})_{54}$ (12 754 Da). Fig. 4 also shows the 1+ charge state of $\text{Au}_{25}(\text{SR})_{18}$ (8549 Da) in both methods. This confirms that the final product in both methods has three Au NMs, namely, $\text{Au}_{144}(\text{SR})_{60}$, $\text{Au}_{137}(\text{SR})_{54}$ and $\text{Au}_{25}(\text{SR})_{18}$. Therefore, these results suggest that DR and Brust methods lead to the same product despite their pathway. The SEC purified DR synthesis product shown in Fig. S3–S6 (ESI[†]) is consistent with the reported studies using the Brust method.^{32,38} Different conditions (temperature, time, *etc.*) and molar ratios are used to synthesize the various sizes of the same thiolate protected Au NMs using the Brust synthesis method.^{34,44} This forms a unique Au nanomolecule series, containing specified number of gold atoms and thiolate ligands. The DR synthesis method used in this report also gave 3 sizes, which is a part of above mentioned Au nanomolecule series.³⁸ The recent publication of $\text{Au}_{\sim 2000}(\text{SR})_{\sim 290}$ provided the largest highly stable unique nanocluster using the Brust method ($\sim 3.8 \text{ nm}^{44}$), which is smaller compared to the normal sizes reported using the DR method.^{23,25–27}

The step-by-step comparison of the synthetic procedure of Brust and DR methods is shown in Scheme 1. The important difference between the two methods is highlighted (red and blue boxes with arrows). Scheme 1 highlights the change in the color of the products inside each reaction flask.

The formation of these nanoclusters is based on a hypothesis from the Brust method,^{7,10,45,46} which was developed based on the color change at every step. Similar Brust-like synthesis in the formation of thiolate protected Ag nanocrystals has also been reported.⁴⁷ In the reported hypothesis, ToABr was used as a phase transfer agent to transfer the Au^{3+} gold salt to an organic phase. Here the color is reddish orange (2nd image on top, Scheme 1) representing the 3+ charge state of Au. Then, the introduction of thiol reduces the 3+ charge state to 1+ forming an $\text{Au}_n(\text{SR})_m$ complex, representing the gradual color change from reddish orange to colorless (3rd image on top, Scheme 1). This is followed by reduction using sodium borohydride produced stable nanoparticles, with a Au(0) core, as indicated by the black color (Scheme 1 rightmost image on top), with a neutral charge state in the core Au atoms. The thermochemical treatment of this obtained crude product converts all the metastable products into highly stable ones. As mentioned in Scheme 1, the major change in DR from Brust is the interchanged steps between the reduction of the mixture (highlighted in blue) and the addition of thiol (highlighted in red). The experimental data backed up by the above mass spectrometry results show that regardless of the change in thiol addition and borohydride reduction steps, both DR and Brust syntheses give the same products. However, the DR procedure contradicts the above-mentioned hypothesis as there is no involvement of thiol in the reduction step, whereas the hypothesis involves the formation of a $\text{Au}_n(\text{SR})_m$ polymer before reduction.

On the other hand, Tong and coworkers reported mechanistic studies on the Brust method, where they argue that even though thiol was added before reduction, the Au–S bond was not formed until the reduction step. They also argue that

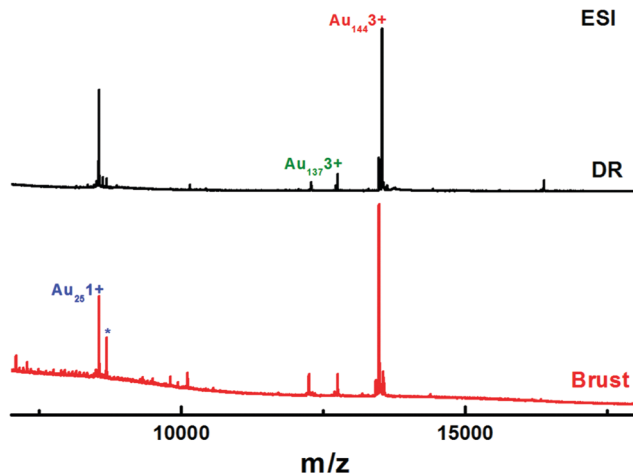


Fig. 4 ESI mass spectrum comparison of dodecanethiol protected atomically precise nanoparticles synthesized using digestive ripening (top) and Brust (bottom) method. (* is Cs^+ adduct.)

instead of the formation of a $\text{Au}_n(\text{SR})_m$ complex, Au forms a complex with ToABr.^{48–52} Meanwhile, one-phase Brust synthesis does not include a phase transfer agent in the synthesis process which could not be explained in the mechanistic study by Tong and coworkers.^{53,54}

Difference between the two methods

As mentioned earlier, the nanoclusters synthesized using the Brust method were highly monodisperse as confirmed by mass spectrometry and single-crystal XRD, and also by their optical properties.^{55,56} Whereas, the DR is used only for synthesizing nanoparticles which are not atomically monodisperse (only size monodisperse).^{26,28,29} However, the above results from three different thiols confirm that through DR, atomic precision is achievable. A keen observation suggests that the precursors used in both methods are the same with one difference: DR uses didodecyldimethylammonium bromide (DDAB) as a phase transfer agent, whereas the Brust method uses tetraoctylammonium bromide (ToABr). The crude product was etched at 80 °C in the Brust synthesis, but in DR, the product was refluxed. Temperature is known to affect the formation of Au NMs.⁵⁷ Here, the Brust synthesis and DR are optimized to obtain the reported Au NMs. A prolonged refluxing results in the decomposition of the products.⁵⁷

To eliminate the influence of the phase transfer agent, the DR method is repeated with a change of phase transfer agent to ToABr. The results are shown in Fig. S9 (ESI[†]) using hexanethiol protected Au NMs. The MALDI spectrum in Fig. S9a (ESI[†]) reveals the presence of a broad peak around 30 kDa with a small peak around 7 kDa and some high mass peaks, similar to the hexanethiol protected Au NMs synthesized using DDAB shown in Fig. 2a. The 30 kDa peaks exactly match with the MALDI spectrum in Fig. 1a explaining the presence of $\text{Au}_{137}(\text{SR})_{54}$ and $\text{Au}_{144}(\text{SR})_{60}$ species, and also 7 kDa species corresponding to $\text{Au}_{25}(\text{SR})_{18}$ similar to Fig. 2a. These $\text{Au}_{144}(\text{SR})_{60}$ and $\text{Au}_{137}(\text{SR})_{54}$ species are confirmed by the ESI-MS spectra in Fig. S9b (ESI[†]),

where the 2+ and 3+ charge states of both $\text{Au}_{144}(\text{SR})_{60}$ and $\text{Au}_{137}(\text{SR})_{54}$ were observed. These observations proved that the change in the phase transfer agent in DR has no impact on the formation of Au NMs. The ToABr has little impact on the relative amounts of the various sizes of Au NMs, but eventually, it leads to the formation of the same Au NMs. Therefore, by keeping all chemicals the same, both DR and Brust syntheses give the same products, regardless of the change in thiol addition and borohydride reduction steps.

Conclusions

In conclusion, this study reveals that digestive ripening can yield atomically precise Au NMs. Atomic precision is achieved by reducing the time difference between the reduction of the mixture and the addition of thiol. The consistency of this process was confirmed using three different thiols. Two aliphatic thiols give $\text{Au}_{25}(\text{SR})_{18}$, $\text{Au}_{137}(\text{SR})_{54}$, and $\text{Au}_{144}(\text{SR})_{60}$, a series of Au NMs with a distinct number of gold and thiolate ligands. The structurally rigid third ligand TBBT, where the sulfur atom is directly attached to the phenyl ring, gives $\text{Au}_{279}(\text{SR})_{84}$, an entirely different series of Au NMs. The comparison of the digestive ripening results with the Brust method results infers that despite major changes in the procedure, both methods lead to the formation of Au NMs. The aliphatic and aromatic series of Au NMs identified in the Brust method are also observed in the DR method. These new findings opened a new path from the long-believed mechanism of the Brust method. This paved a way for future work on the study of the underlying mechanism for the formation of Au NMs, which should satisfy both pathways. The DR result using ToABr eliminates the influence of any difference in the chemicals and reiterates that Brust and DR methods yield the same Au NMs despite the difference in their pathways.

Experimental

Materials

Hydrogen tetrachloroaurate(III) trihydrate ($\text{HAuCl}_4 \cdot 3\text{H}_2\text{O}$) (Alfa aesar, 99.99%), tetraoctylammonium bromide (ToABr) (Aldrich, 98%), didodecyldimethylammonium bromide (DDAB) (Acros, 99%), sodium borohydride (NaBH_4 , 99%), 4-*tert*-butylbenzenethiol (TBBT)(TCI, 99%), 1-dodecanethiol (Acros, 98%), 1-hexanethiol (Aldrich), cesium acetate (Acros, 99%), and *trans*-2-[3(4-*tert*-butylphenyl)-2-methyl-2 propenylidene]malononitrile (DCTB matrix) (Fluka \geq 99%) were used in this study. HPLC grade solvents such as tetrahydrofuran, toluene, and methanol were obtained from Fisher Scientific. All the materials were used as received.

Synthesis

The synthesis was performed based on a previous report.²⁶ The synthesis method comprises 2 parts. First, didodecyldimethylammonium bromide (DDAB) (110 mg) was dissolved in toluene. Then, $\text{HAuCl}_4 \cdot 3\text{H}_2\text{O}$ (40 mg) was added to the above solution and transferred to a round bottom flask (RBF).

Typically, $\text{HAuCl}_4 \cdot 3\text{H}_2\text{O}$ does not dissolve in toluene, but using DDAB as a phase transfer agent, it can be dissolved in toluene. The solution was stirred for 15 minutes by thorough mixing. The mixture was then reduced by NaBH_4 (18 mg) in water, which is indicated by the solution turning black. After 30 seconds, hexanethiol (0.43 mL) ($\text{Au} : \text{thiol} = 1 : 30$) was added rapidly, and the solution was stirred for 1 hour. The same thiol ratio was maintained in the reaction as with the other two thiols. Second, the RBF was connected to a refluxing condenser and refluxed for 18 hours. Finally, the refluxing was stopped, and the temperature was allowed to reach room temperature. The solution was rotary evaporated to remove the excess solvent. The resulting product was washed with methanol and water mixture (3–4 times) to remove excess thiol and by-products. The same method was repeated by only changing the phase transfer agent to ToABr for comparison with the Brust method.

The Brust synthesis was carried out by small changes in the Brust⁷ two-phase synthesis. First, ToABr (0.14 g) was dissolved in toluene (7.5 mL) in an RBF. Then, $\text{HAuCl}_4 \cdot 3\text{H}_2\text{O}$ (0.1 g) was dissolved in distilled water (10 mL) and added to the toluene solution. The mixture was stirred for 30 minutes. The colour of the organic phase changed to bright orange, indicating that the phase transfer was complete. Water was discarded. The whole setup was transferred to an ice bath and stirring was continued for 30 minutes. 120 μL of 1-dodecanethiol ($\text{Au} : \text{thiol} = 1 : 2$) was added and the stirring was continued for another 30 minutes. The solution turned white. The mixture was reduced by NaBH_4 (0.1 mg) in 5 mL of ice-cold water, and immediately the colour changed to black. The solution was further stirred for 3 hours. Then, the solvent was removed from the product and washed with a water–methanol mixture 3 times, and the resulting crude was separated. The crude product was redistributed in toluene (1 mL) with an excess amount of 1-dodecanethiol and etched at 80 °C for 2 days. The resulting product was washed with a water–methanol mixture, and the final product was obtained.

Conflicts of interest

There are no conflicts to declare.

Acknowledgements

NSF-CHE-1808138 supported the performed work. We acknowledge Institute for Imaging and Analytical Technology (I²AT) at Mississippi State University and Rooban Venkatesh K G Thirumala for the support in TEM image collection.

Notes and references

- 1 A. C. Templeton, W. P. Wuelfing and R. W. Murray, *Acc. Chem. Res.*, 2000, **33**, 27–36.
- 2 D. J. Barber and I. C. Freestone, *Archaeometry*, 1990, **32**, 33–45.
- 3 E. L. Downs and D. R. Tyler, *Coord. Chem. Rev.*, 2014, **280**, 28–37.
- 4 J. Fang, B. Zhang, Q. Yao, Y. Yang, J. Xie and N. Yan, *Coord. Chem. Rev.*, 2016, **322**, 1–29.
- 5 S. Sun, P. Mendes, K. Critchley, S. Diegoli, M. Hanwell, S. D. Evans, G. J. Leggett, J. A. Preece and T. H. Richardson, *Nano Lett.*, 2006, **6**, 345–350.
- 6 P. A. Schaal, A. Besmehn, E. Maynicke, M. Noyong, B. Beschoten and U. Simon, *Langmuir*, 2012, **28**, 2448–2454.
- 7 M. Brust, M. Walker, D. Bethell, D. J. Schiffrin and R. Whyman, *J. Chem. Soc., Chem. Commun.*, 1994, 801–802.
- 8 M. W. Heaven, A. Dass, P. S. White, K. M. Holt and R. W. Murray, *J. Am. Chem. Soc.*, 2008, **130**, 3754–3755.
- 9 P. D. Jadzinsky, G. Calero, C. J. Ackerson, D. A. Bushnell and R. D. Kornberg, *Science*, 2007, **318**, 430–433.
- 10 T. G. Schaaff and R. L. Whetten, *J. Phys. Chem. B*, 1999, **103**, 9394–9396.
- 11 R. L. Whetten, J. T. Khoury, M. M. Alvarez, S. Murthy, I. Vezmar, Z. L. Wang, P. W. Stephens, C. L. Cleveland, W. D. Luedtke and U. Landman, *Adv. Mater.*, 1996, **8**, 428–433.
- 12 N. A. Sakthivel, S. Theivendran, V. Ganeshraj, A. G. Oliver and A. Dass, *J. Am. Chem. Soc.*, 2017, **139**, 15450–15459.
- 13 C. Zeng, Y. Chen, K. Kirschbaum, K. Appavoo, M. Y. Sfeir and R. Jin, *Sci. Adv.*, 2015, **1**, e1500045.
- 14 C. Zeng, H. Qian, T. Li, G. Li, N. L. Rosi, B. Yoon, R. N. Barnett, R. L. Whetten, U. Landman and R. Jin, *Angew. Chem., Int. Ed.*, 2012, **51**, 13114–13118.
- 15 D. Crasto and A. Dass, *J. Phys. Chem. C*, 2013, **117**, 22094–22097.
- 16 D. Crasto, S. Malola, G. Brosofsky, A. Dass and H. Häkkinen, *J. Am. Chem. Soc.*, 2014, **136**, 5000–5005.
- 17 H. Yang, Y. Wang, A. J. Edwards, J. Yan and N. Zheng, *Chem. Commun.*, 2014, **50**, 14325–14327.
- 18 S. G. Booth, A. Uehara, S. Y. Chang, C. La Fontaine, T. Fujii, Y. Okamoto, T. Imai, S. L. M. Schroeder and R. A. W. Dryfe, *Chem. Sci.*, 2017, **8**, 7954–7962.
- 19 Y. Cao, T. Liu, T. Chen, B. Zhang, D.-E. Jiang and J. Xie, *Nat. Commun.*, 2021, **12**, 3212.
- 20 A. Bhakta and E. Ruckenstein, *J. Chem. Phys.*, 1995, **103**, 7120–7135.
- 21 I. M. Lifshitz and V. V. Slyozov, *J. Phys. Chem. Solids*, 1961, **19**, 35–50.
- 22 C. Wagner, *Z. Elektrochem., Ber. Bunseng. Phys. Chem.*, 1961, **65**, 581–591.
- 23 X. Lin, C. Sorensen and K. Klabundea, *J. Nanopart. Res.*, 2000, **2**, 157–164.
- 24 D. Jose and B. R. Jagirdar, *J. Phys. Chem. C*, 2008, **112**, 10089–10094.
- 25 J. R. Shimpfi, D. S. Sidhaye and B. L. V. Prasad, *Langmuir*, 2017, **33**, 9491–9507.
- 26 J. Seth and B. L. V. Prasad, *Nano Res.*, 2016, **9**, 2007–2017.
- 27 P. Sahu and B. L. V. Prasad, *Nanoscale*, 2013, **5**, 1768–1771.
- 28 B. L. V. Prasad, S. I. Stoeva, C. M. Sorensen and K. J. Klabunde, *Langmuir*, 2002, **18**, 7515–7520.

- 29 M.-L. Lin, F. Yang and S. Lee, *Colloids Surf.*, 2014, **448**, 16–22.
- 30 P. Sahu and B. L. V. Prasad, *Chem. Phys. Lett.*, 2012, **525–526**, 101–104.
- 31 P. Wang, X. Qi, X. Zhang, T. Wang, Y. Li, K. Zhang, S. Zhao, J. Zhou and Y. Fu, *Nanoscale Res. Lett.*, 2017, **12**, 25.
- 32 H. Qian and R. Jin, *Chem. Mater.*, 2011, **23**, 2209–2217.
- 33 A. Dass, A. Stevenson, G. R. Dubay, J. B. Tracy and R. W. Murray, *J. Am. Chem. Soc.*, 2008, **130**, 5940–5946.
- 34 C. Kumara, X. Zuo, J. Ilavsky, K. W. Chapman, D. A. Cullen and A. Dass, *J. Am. Chem. Soc.*, 2014, **136**, 7410–7417.
- 35 M. Zhu, E. Lanni, N. Garg, M. E. Bier and R. Jin, *J. Am. Chem. Soc.*, 2008, **130**, 1138–1139.
- 36 Z. Luo, V. Nachammai, B. Zhang, N. Yan, D. T. Leong, D.-E. Jiang and J. Xie, *J. Am. Chem. Soc.*, 2014, **136**, 10577–10580.
- 37 V. R. Jupally, A. C. Dharmaratne, D. Crasto, A. J. Huckaba, C. Kumara, P. R. Nimmala, N. Kothalawala, J. H. Delcamp and A. Dass, *Chem. Commun.*, 2014, **50**, 9895–9898.
- 38 M. Rambukwella, N. A. Sakthivel, J. H. Delcamp, L. Sementa, A. Fortunelli and A. Dass, *Front. Chem.*, 2018, **6**, 330.
- 39 N. A. Sakthivel and A. Dass, *Acc. Chem. Res.*, 2018, **51**, 1774–1783.
- 40 S. Knoppe, J. Boudon, I. Dolamic, A. Dass and T. Bürgi, *Anal. Chem.*, 2011, **83**, 5056–5061.
- 41 N. A. Sakthivel, V. R. Jupally, S. K. Eswaramoorthy, K. H. Wijesinghe, P. R. Nimmala, C. Kumara, M. Rambukwella, T. Jones and A. Dass, *Anal. Chem.*, 2021, **93**, 3987–3996.
- 42 N. K. Chaki, Y. Negishi, H. Tsunoyama, Y. Shichibu and T. Tsukuda, *J. Am. Chem. Soc.*, 2008, **130**, 8608–8610.
- 43 Y. Shichibu, Y. Negishi, T. Tsukuda and T. Teranishi, *J. Am. Chem. Soc.*, 2005, **127**, 13464–13465.
- 44 S. Vergara, U. Santiago, C. Kumara, D. Alducin, R. L. Whetten, M. Jose Yacaman, A. Dass and A. Ponce, *J. Phys. Chem. C*, 2018, **122**, 26733–26738.
- 45 S. Chen, A. C. Templeton and R. W. Murray, *Langmuir*, 2000, **16**, 3543–3548.
- 46 Y.-S. Shon, C. Mazzitelli and R. W. Murray, *Langmuir*, 2001, **17**, 7735–7741.
- 47 J. García-Barrasa, J. M. López-de-Luzuriaga, M. Monge, K. Soulantica and G. Viau, *J. Nanopart. Res.*, 2011, **13**, 791–801.
- 48 Y. Li, O. Zaluzhna and Y. J. Tong, *Langmuir*, 2011, **27**, 7366–7370.
- 49 Y. Li, O. Zaluzhna, B. Xu, Y. Gao, J. M. Modest and Y. J. Tong, *J. Am. Chem. Soc.*, 2011, **133**, 2092–2095.
- 50 O. Zaluzhna, Y. Li, T. C. Allison and Y. J. Tong, *J. Am. Chem. Soc.*, 2012, **134**, 17991–17996.
- 51 O. Zaluzhna, Y. Li, C. Zangmeister, T. C. Allison and Y. J. Tong, *Chem. Commun.*, 2012, **48**, 362–364.
- 52 P. J. G. Goulet and R. B. Lennox, *J. Am. Chem. Soc.*, 2010, **132**, 9582–9584.
- 53 A. Dass, T. Jones, M. Rambukwella, D. Crasto, K. J. Gagnon, L. Sementa, M. De Vetta, O. Baseggio, E. Aprà, M. Stener and A. Fortunelli, *J. Phys. Chem. C*, 2016, **120**, 6256–6261.
- 54 T. C. Jones, L. Sumner, G. Ramakrishna, M. B. Hatshan, A. Abuhagr, S. Chakraborty and A. Dass, *J. Phys. Chem. C*, 2018, **122**, 17726–17737.
- 55 M. S. Devadas, J. Kim, E. Sinn, D. Lee, T. Goodson and G. Ramakrishna, *J. Phys. Chem. C*, 2010, **114**, 22417–22423.
- 56 S. Knoppe and T. Bürgi, *Acc. Chem. Res.*, 2014, **47**, 1318–1326.
- 57 T. Chen, Q. Yao, X. Yuan, R. R. Nasaruddin and J. Xie, *J. Phys. Chem. C*, 2017, **121**, 10743–10751.